Photocrosslinking silver nanoparticles–aloe vera–silk fibroin composite hydrogel for treatment of full-thickness cutaneous wounds

Yangkun Liu[1,†], JinChuan Fan[1,†], MingQi Lv[1,†], Kepeng She[1], Jiale Sun[1], Qingqing Lu[1], Changhao Han[1], SongTao Ding[1], Shuang Zhao[1,2], GuiXue Wang[2,*], YuChan Zhang[1,*] and GuangChao Zang[1,*]

[1]Institute of Life Science, And Laboratory of Tissue and Cell Biology, Lab Teaching & Management Center, Chongqing Medical University, Chongqing 400016, China and [2]Key Laboratory for Biorheological Science and Technology of Ministry of Education, State and Local Joint Engineering Laboratory for Vascular Implants, Bioengineering College of Chongqing University, Chongqing 400030, China

*Correspondence address. E-mail: Zhangyc@cqmu.edu.cn (Y.Z.); E-mail: wanggx@cqu.edu.cn (G.W.);
E-mail: zangguangchao@cqmu.edu.cn (G.Z.)
[†]These authors contributed equally to this work.
Received 20 July 2021; revised 5 August 2021; accepted on 11 August 2021

Abstract

Damage to the skin causes physiological and functional issues. The most effective treatment approach is the use of wound dressings. Silk fibroin (SF) is a promising candidate biomaterial for regulating wound healing; however, its antibacterial properties and biological activity must be further improved. In this study, a photocrosslinking hydrogel was developed to treat full-thickness cutaneous wounds. The composite hydrogel (Ag–AV–SF hydrogel) was prepared by introducing the silver nanoparticles (AgNPs) and aloe vera (AV) as the modifiers. *In vitro* study exhibited great antibacterial ability, biocompatibility and cell-proliferation and -migration-promoting capacities. It also showed the pH-response releasing properties which release more AgNPs in a simulated chronic infection environment. The healing effect evaluation *in vivo* showed the healing-promoting ability of the Ag–AV–SF hydrogel was stronger than the single-modifiers groups, and the healing rate of it reached 97.02% on Day 21, higher than the commercial wound dressing, silver sulfadiazine (SS) cream on sale. Additionally, the histological and protein expression results showed that the Ag–AV–SF hydrogel has a greater effect on the pro-healing regenerative phenotype with M2 macrophages at the early stage, reconstructing the blood vessels networks and inhibiting the formation of scars. In summary, the Ag–AV–SF hydrogel developed in this study had good physical properties, overwhelming antibacterial properties, satisfactory biocompatibility and significantly promoting effect on cell proliferation, migration and wound healing. Overall, our results suggest that the Ag–AV–SF hydrogel we developed has great potential for improving the wound healing in clinical treatment.

Keywords: silk fibroin; silver nanoparticles; aloe vera; hydrogel; wound healing

Introduction

The skin plays a vital role in protecting the body from external mechanical damage, acting as the first barrier against the outside environment. Skin injuries will lead to critical physiological and functional disturbances [1, 2]. Wound healing is a complex process that includes four primary steps: hemostasis, inflammation, proliferation and remodeling [3]. The wrong treatment will cause chronic inflammation at the site of an injury and eventually impede fibroblast migration and

(Extracellular Matrix)ECM formation, slowing the healing process [4]. Therefore, an effective skin wound healing treatment is sorely needed, the key to which is developing a suitable skin wound dressing that can accelerate wound healing through simple techniques [5].

An advanced multifunctional dressing for wound healing must be biocompatible, resistant to the outer environment, provide a moist surrounding for healing, be air-penetrable and be simple to withdraw without any bio-toxicity or secondary injuries. Based on these standards, many types of wound dressings have been developed using natural materials, synthetic materials or a mixture of both [6, 7].

Among the natural biomaterials, silk fibroin (SF) has attracted the most research attention nowadays. SF has already been applied for wound repair owing to its biocompatibility, weak immunogenic effects, non-toxicity, mechanical toughness, controllable biodegradability and cost-effectiveness [8, 9]. Meanwhile, the tripeptide Arg-Gly-Asp (RGD) sequence of SF can support cell adhesion, proliferation and migration of various cell types, including epithelial cells, endothelial cells and fibroblasts [10, 11]. In many application forms, hydrogel is the most appropriate form for SF in wound dressings because it could easily attach to the skin without adhesives. Many types of hydrogels were developed based on SF via various strategies. A SF hydrogel loaded with fibroblast growth factor was developed and applied for promoting wound full-thickness skin excision via sonication, a direct and simple way to form β-sheets [12]. Jing *et al.* [13] reported a (Tannins Acid) TA gelatin-enhanced SF–TA hybrid hydrogel based on a chemical crosslinking method which exhibited remarkable antimicrobial and antioxidant activities for improving wound healing.

Although SF has exhibited excellent application potential as a wound dressing, it has poor antibacterial properties when utilized on wounds by itself. Therefore, improving the antibacterial properties of SF is necessary [14]. Silver nanoparticles (AgNPs) are natural antimicrobial agents with broad spectrum antimicrobial properties and strong permeability [15]. AgNP-coated silk-based biomaterials have been reported to exhibit satisfying antibacterial activity against *Escherichia coli* (*E. coli*) and *Staphylococcus aureus* (*S. aureus*) [16, 17]. Furthermore, the high affinity between the human body and SF hydrogel could ensure that nanoparticles encapsulated in SF permeate from the outermost of the corneum to the inner [18]. Except for antimicrobial activities, wound healing ability of SF can be enhanced using bioactive ingredients. Aloe vera (AV) has already been applied in many fields since the ancient Roman era or even before [19], consisting of tannin, saponin, flavonoids, steroids, glucomannan and glucose-6-phosphate, with promising wound-healing potential to stimulate the proliferation and migration of fibroblasts by affecting the fibroblast growth factor [20, 21].

Considering the aforementioned factors, we fabricated a composite bio-hydrogel through photocrosslinking in this study and used it to treat full-thickness cutaneous wounds (Fig. 1). Ag–AV–SF hydrogel shows great potential in wound healing. The loose and porous structure provides abundant sites for cell adhesion, and the strength of internal chemical bonds is also significantly enhanced. It also showed the pH-response releasing property which releases more AgNPs in a simulated chronic infection environment. Cell biology experiments have shown that the hydrogel could promote the proliferation and migration of fibroblasts *in vitro*. *In vivo*, the hydrogel treatment group exhibit greater healing effect than other parallel control groups, and the wound healing rate reached 97.02% in the same period. Histological analysis shows the prepared hydrogel effectively inhibits the inflammatory response and promotes the reconstruction of the vascular network at the wound site. Meanwhile, the higher expression of IL-10 implied the Ag–AV–SF hydrogel has more effects on the pro-healing regenerative phenotype with M2 macrophages at the early stage. Finally, the protein expression level results indicate that the therapeutic produced by the hydrogel is scar-less wound healing. Hence, this study expects to deal with the future clinical healing issue.

Experiment section

Preparation of Ag–AV–SF hydrogel

The SF solution was prepared according to a previously reported method [22]. After obtaining the SF solution, it was subsequently centrifuged to remove silk aggregates. The final concentration of SF was adjusted to 5.0 wt% with deionized water. The Ag–SF, AV–SF and Ag–AV–SF hydrogels were prepared by mixing Ag NO_3, AV and both with SF solution, respectively. The three pre-hydrogel solutions were then illuminated (40 W) for 24 h in culture dishes to obtain the different hydrogels [23]. To ensure the lowest possible biotoxicity and the potential for all Ag(I) to be reduced to Ag (0), the concentration of $AgNO_3$ was set to 0.5 mg/ml. The suitable concentration of AV is screened via Cell Counting Kit-8 (CCK-8) assay. Briefly, L929 cells were seeded in a 96-well plate, and different concentrations of AV solutions were applied as stimulating factors. After stimulating for 24 h, the absorbance values were determined for the optimal concentration of different dispersions (Fig. S1).

Physical properties of the hydrogel

Micromorphology

The micromorphology of the AgNPs was observed using scanning electron microscopy (SEM, SU8010, Hitachi, Ltd., Japan) after freeze-drying. The diameter of the AgNPs was observed by transmission electron microscopy (TEM, 7500, Hitachi, Ltd., Japan).

Fourier transform infrared spectroscopy spectra

Fourier transform infrared spectroscopy spectra (FTIR) (Thermo Fisher Scientific-CN, USA) was analyzed in 4000–400 cm^{-1} to verify the binding functional groups in the hybrid system of the Ag–AV–SF hydrogel.

Thermogravimetric analysis

Thermogravimetric analysis (TGA) is a physicochemical property that could be treated as the colloidal stability of the hydrogel [24, 25]. TGA was performed using a thermal gravimetric analyzer (TA SDT 650, TA, USA). The measurements were tested using the standard mode and the temperature was set to increase from room temperature to 500°C at a heating rate of 20°C·min^{-1}.

Swelling and tissue adhesion test

Swelling and adhesion test were conducted to assess the attachment ability of the Ag–AV–SF hydrogel. The hydrogel was blended with FITC and then smeared on a piece of porcine skin which was then covered with another piece of porcine skin. The pieces were frozen sliced after being kept at room temperature for 1 h and 24 h. Finally, they were observed using fluorescence microscopy [26]. The Ag–AV–SF hydrogels (150 μL) were coated between two porcine skin pieces (1.5 × 4.5 cm^2). One end of the porcine skin was tightened with a rubber band and the other end was fixed using a heavy object. The test was operated according to Fig. S2a. The maximum weight after fitting can be used to evaluate the adhesion ability.

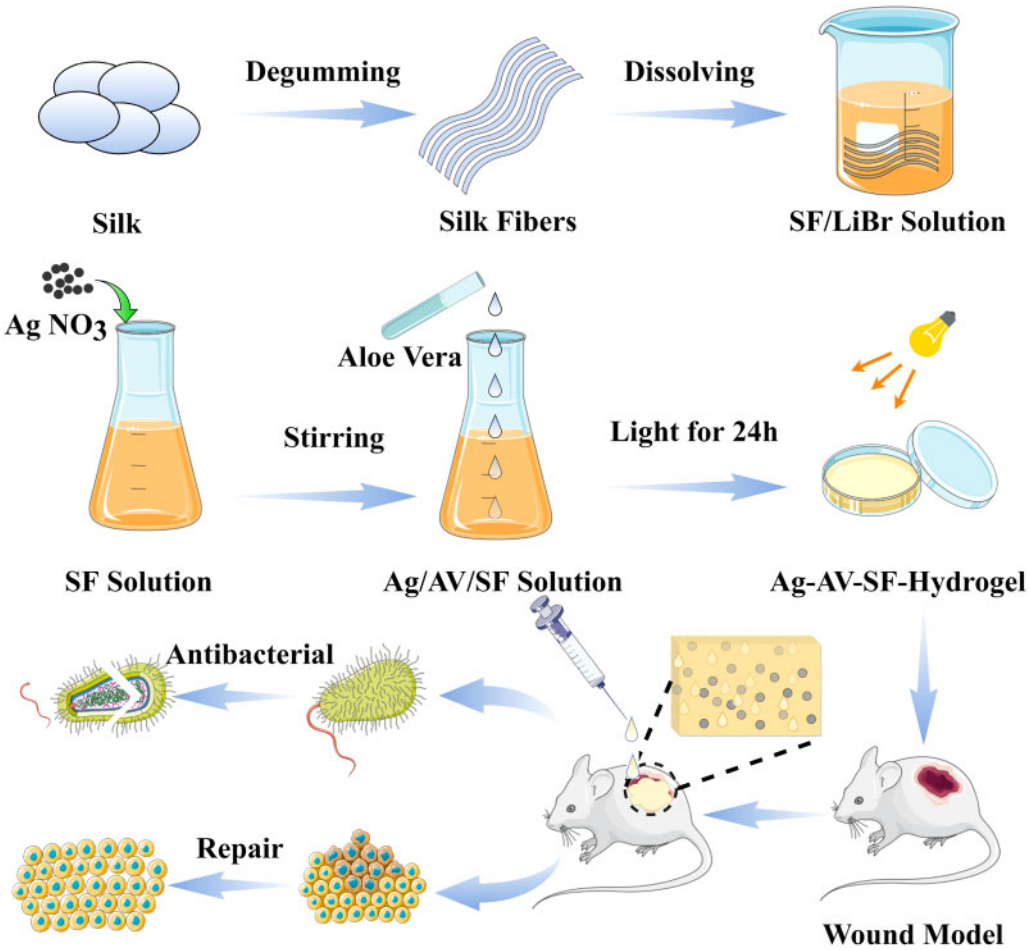

Figure 1. Ag-AV-SF hydrogel was prepared via photocrosslinking approach and applied in wounded rat models for antibacterial and repair

Ag+ release rate of the Ag–AV–SF hydrogel

The release mass of Ag+ was detected using an inductively coupled plasma source mass spectrometer (Agilent7900, USA). The pH of choric wound was reported to be around 6.5 [27], so we operated the release test in both neutral (pH = 7.4) and acidic (pH = 6.5) environments. The Ag–AV–SF hydrogel was dialyzed (3500 MW) at room temperature and the detection samples were collected from Days 1–5. The release rate was finally calculated using the following equation

$$Releaserate(\%) = \frac{M1}{D} \times 100\%$$

(M1 refers to the total release mass of Ag, D refers to the detection time points)

Antibacterial assays

Gram-positive *S. aureus* and Gram-negative *E. coli* were used as the model bacteria. The antibacterial activity of different hydrogels was assessed through a modified disc diffusion test (K-B)method. Agar plates were prepared and inoculated with the aforementioned bacteria which were seperated into 4 groups to test SF, Ag-SF, AV-SF, and Ag-AV-SF hydrogels respectively. The four hydrogels were applied to the corresponding areas, and the diameter of the hydrogel was controlled at 6 mm. The diameters of the antibacterial rings were measured to evaluate the antibacterial capacity after incubation at 37°C for 24 h [28].

Cytotoxicity of L929

Fibroblasts are a type of skin cells, more closely associated skin and wound healing than (Mesenchymal Stem Cells) MSCs [29], so it was chosen as the model cell in this study. The cells were all cultured in (Dulbecco's Modified Eagle Medium) DMEM containing 1% (Penicillin-Streptomycin)P/S solution and 10% (Fetal Bovine Serum)FBS at 37°C in 5% CO_2. The cytotoxicity of different hydrogels was detected using a CCK-8 assay. The L929 cells were cultured on a 96-well plate (5000/each), then treated with the four pre-hydrogel solutions (10 µl/each) for 24 h. The absorbances values were then measured at 450 nm using a spectrophotometer (Thermo Fisher Scientific-CN, USA) to evaluate the cytotoxicity [30].

Cell proliferation and migration *in vitro*

After seeding cells onto six-well plates for 24 h, the original medium was discarded and replaced with a fresh medium (control), along with the medium containing SF, Ag–SF, AV–SF or Ag–AV–SF pre-hydrogel solutions for another 24 h. Actin staining was carried out to visualize the cytoskeleton through the FITC-conjugated Phalloidin and DAPI was used to stain the cell nuclei.

Cells were seeded onto the six-well plate and incubated until the cells were fully covered. A gap of about 150 µm was drawn, and then washed with PBS for three times. To study only the effect of hydrogel on cell migration, the culture medium was changed into a serum-free medium, due to serum starvation, environment was

reported as another way used to suppress cell proliferation [31, 32]. The initial wounding and the migration of cells in the scratched area were photographically monitored after 12 h.

Wound healing assay

After anesthetization using an aesthesia machine with isoflurane volatiles (RWD Life Science, Shenzhen, China), the dorsal surface hairs of adult rats (8 weeks) were shaved and a square wound ($S = 1\ cm^2$) or circle piece ($D = 1$ cm) of skin was removed from the back. Before treatment with different hydrogels, iodoform and alcohol were used to avoid infection and the rats in the control group were only treated with iodoform and alcohol. Different hydrogels with a weight of 0.5 g were applied to the wound surface of the rats to ensure complete coverage of the wound, in addition, the final mass of AgNPs on the wounds is about 1.25 mg and the AV is about 7.5 mg. The various hydrogel dressings were replaced 2 days apart according to a clinical case reported in Tissue Repair Professional Committee of Traumatology Branch of Chinese Medical Association. The experimental protocol and operation were approved by the Ethic Committee of Chongqing Medical University. The animals in this experiment were all under humane care.

Comparison with single modifier and SS

Rats were randomly divided into five groups ($n = 9$). Iodoform and alcohol were then used to avoid infection, after which the wounds were covered by SF-hydrogel, Ag–SF hydrogel, AV–SF hydrogel and Ag–AV–SF hydrogel. Photographs of the wound areas were taken on the 7th, 14th and 28th days. Tissue samples along with 0.5 cm of normal skin were taken on the 7th and 28th days. Subsequently, three other groups ($n = 9$) of rats were treated as mentioned above. Differently, the wounds were covered by the silver sulfadiazine (SS) cream and Ag–AV–SF hydrogel. Photographs of the wound areas were taken on the 7th, 14th and 21st days. Tissue samples along with 0.5 cm normal skin were taken on the 7th and 21st days.

Histological analysis

To evaluate the healing promotion *in vivo*, wound tissues, along with 0.5 cm of normal skin, were obtained at different time points post-surgery for histological evaluation. (Hematoxylin - Eosin)HE staining was utilized to evaluate the wound beds at different times. The immunohistochemical (IHC) staining of CD68, CD31, (Mannose Receptor 1)MRC1 and (Proliferating Cell Nuclear Antigen)PCNA were performed to study the effect of the immunoreactions, neovascularization and cell proliferation *in vivo* on the wounds. Masson staining was operated to assess the collagen deposition.

Biosecurity *in vivo*

After anesthetization, the SD rats' dorsal surface hairs were shaved and a piece of $0.5 \times 0.5\ cm^2$ skin was removed. The FITC-labeled Ag–AV–SF hydrogel was smeared on the wound. The diffusion range was recorded by using a multifunction laser-scanning system after 0, 4, 12 and 24 h. In addition, the organs including hearts, brains, spleens, lungs, kidneys, testicles and livers were obtained after treated for 28 days to assess the biosecurity by HE staining.

Detection of protein expression level

A western blot assay was carried out to assess the expression level of TGF-β3 and TGF-β1 to study the anti-scaring and pro-scaring effects. The expression level of VEGF and IL-10 were used to verify the macrophage transformation from the M1 phenotype to M2.

The details regarding the materials and reagents used are provided in the supplementary information.

Results

Preparation and characterization of different hydrogels

The pre-hydrogel solution (Fig. 2a) was successfully transferred into a thick and dark yellow hydrogel (Fig. 2b), and the hydrogel was attached to the bottom of the receptacle after it was illuminated. The SEM micrographs of the Ag–AV–SF hydrogel showed that the internal structure of the hydrogel is porous and the pore size is around 100 μm (Fig. 2c and d). AgNPs were characterized by SEM and TEM, where the prepared AgNPs scattered onto the proteins proving that the AgNPs obtained in the combined system are reduced *in-situ* by SF and the size of AgNPs is around 40 nm (Fig. 2e and f). Subsequently, we utilized the Ag–AV–SF hydrogel to depict the acronym of Chongqing Medical University (CQMU) onto glass blending with hematochrome to demonstrate the excellent plasticity of the hydrogel (Fig. 2g). The characteristic peaks in the EDX spectrums of the Ag–AV–SF hydrogel (Fig. 2h) indicate that the SF successfully plays its role to reduction and attach AgNPs onto the hydrogel surface.

Tight binding between functional groups and continuous release of Ag

FTIR was used to analyze the binding of the functional groups inside the differently prepared hydrogels. As shown in Fig. 3a, C–N stretching ($1451.88\ cm^{-1}$) in the SF transferred into the new C–N ($1017.68\ cm^{-1}$); at the same time, the intensity of C–O ($3339.11\ cm^{-1}$), C = O ($1634.70\ cm^{-1}$ and $1249.80\ cm^{-1}$) and N–H stretching ($1543.73\ cm^{-1}$) in the Ag–AV–SF system significantly improved compared with that in the SF [25]. The phenomenon of stretching vibration was attributed to the α-amino nitrogen and α-carboxylic oxygen from the tyrosine formed complexes with silver ions through coordination bonds [33]. When the temperature increased from room temperature to 500°C, the relative mass of the Ag–AV–SF hydrogel remained higher than the rest, and was maintained throughout the entire process (Fig. 3b). The TGA results showed that the Ag–AV–SF hydrogel had excellent thermostability indicating that the integrity of the structure was maintained under the conditions of preservation and practical application. The thermal properties of the Ag–AV–SF hydrogel showed great improvement for synergistic effect [34]. The Ag+ release rate in neutral (pH = 7.4) and acidic environment (pH = 6.5) for 5 days is shown in Fig. 3c. The relative release mass of AgNPs reached 40.89% in neutral environment, and reached 55.12% in acidic environment, indicating that the hydrogel showed a pH-response property. In this case, the hydrogel ensured that upon infection, as the pH levels turn acidic, it would release more AgNPs to resist bacterial and inhibit the immune reaction. The properties above imply that the prepared Ag–AV–SF hydrogel has superior structure stability and the loading capacity of nanoparticles, ensuring the performance of its antibacterial function consistently and steadily.

Swelling and tissue adhesion test

Swelling and tissue adhesion properties are the additive attributes aiming to verify that the hydrogel will fill the wound and would not fall out when applied (Fig. S2). These outcomes indicate that the hybrid hydrogel can adhere to the surrounding tissue tightly, protecting the wound tissue from the outside environment.

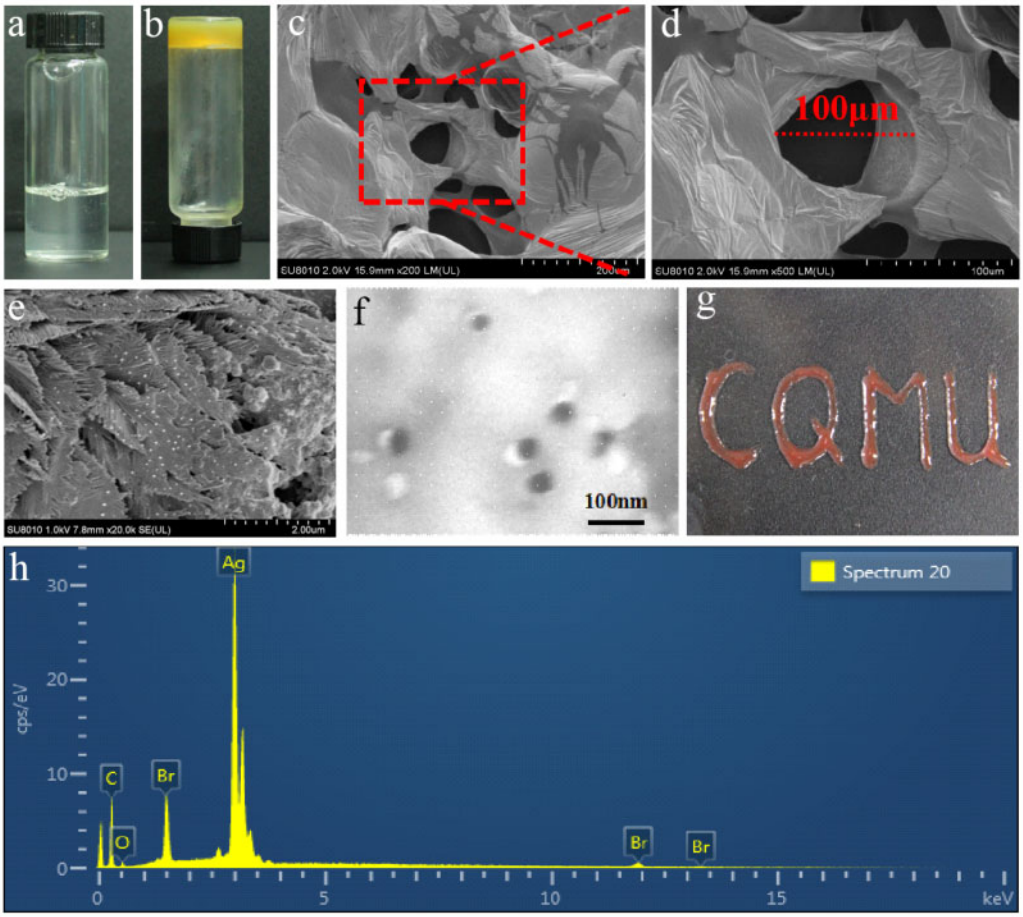

Figure 2. (a) The pre-hydrogel solution of the composite hydrogel, (b) the final hydrogel, (c–e) the SEM image of the hydrogel after frozen dry and dried at room temperature, (f) the TEM of the AgNPs, (g) the acronym of Chongqing Medical University (CQMU) shaped using the Ag–AV–SF hybrid hydrogel and (h) the EDX spectrum of the AgNPs and elements mapping of the Ag–AV–SF hydrogel

Antibacterial properties against *E. coli* and *S. aureus*

The intrusion of bacteria and microorganisms in a wound is the main cause of severe chronic infections. *Escherichia coli* and *S. aureus* are the most representative model bacteria. The results of the antibacterial rings are shown in Fig. 4a, and the statistical analyses are given in Fig. 4b and c. Apparently, the antibacterial rings presented in the Ag–AV–SF hydrogel had the largest diameter both for *E. coli* (13.92 ± 0.94 mm) and *S. aureus* (10.623 ± 0.61 mm). Meanwhile, the Ag–SF group and the AV–SF group showed a significant difference compared with the Ag–AV–SF-treated group, implying that the Ag–AV–SF hydrogel presents superior antibacterial properties than other groups and the Ag–AV–SF hydrogel combines the AgNPs' and AV's antimicrobial properties and demonstrating synergistic effects.

Cell proliferation and migration *in vitro*

Fibroblasts play a crucial role in the proliferative phase of wound healing [35]. Fluorescence staining of L929 cells was conducted to assess the proliferation-promoting capability of the Ag–AV–SF hydrogel (Fig. 5a). After adding the pre-hydrogel solution for 24 h, the nucleus and cytoskeleton of the Ag–AV–SF hydrogel-treated group vary the most in comparison to the other groups, indicating the Ag–AV–SF hydrogel has a better effect on cell proliferation. Furthermore, the CCK-8 assay showed that the cell proliferation-promoting capacity of the Ag–AV–SF hydrogel was more overwhelming than the others (Fig. 5b). Next, the scratch test was conducted to study the cell-migration capacity. As shown in Fig. 5c, the gap with the Ag–AV–SF hydrogel reduced the most compared with other groups. Ag–AV–SF hydrogel effectively promoted cell proliferation and migration providing the fundamental for wound healing.

In vivo wound-healing evaluation

After studying the cell proliferation and migration, wounded rats were established to verify the healing effects *in vivo*. The wound healing statuses of different modifiers are shown in Fig. 6a and b. Ag–AV–SF hydrogel showed the most obvious area reduction, indicating that compared with the single modifier, Ag–AV–SF hydrogel displayed a synergistic effect of the three materials, and showed better repair effect than them. On the 7th day, the area of the wound showed significant reduction, as the Ag–AV–SF hydrogel inhibited inflammatory reactions in early stages of healing. On the 14th day, the healing area of the group treated with the Ag–AV–SF hydrogel decreased more than other groups, indicating that the Ag–AV–SF hydrogel has good antibacterial properties in the middle period of wound repair. On the 28th day, the extent of the wound treated with the Ag–AV–SF hybrid hydrogel was nearly completely closed (98.79%),

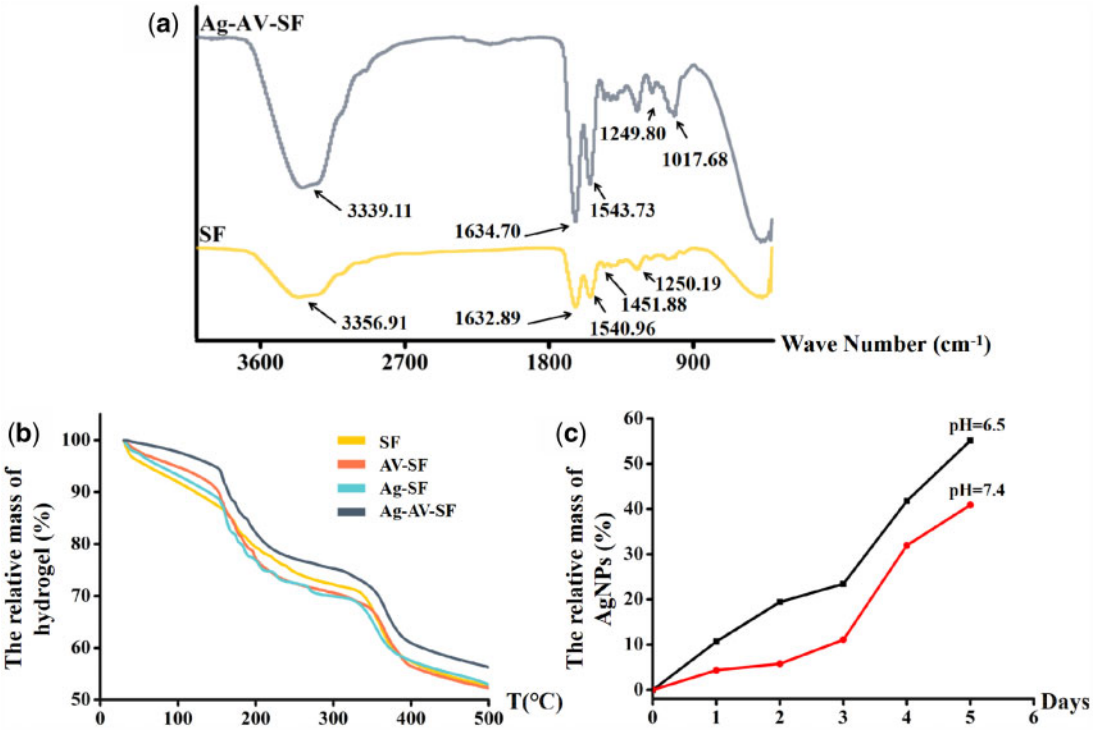

Figure 3. (a) The FTIR of SF hydrogel and Ag–AV–SF hydrogel, (b) the TGA of four types of hydrogels and (c) the release rate of Ag in neural (pH = 7.4) and acidic (pH = 6.5) environments

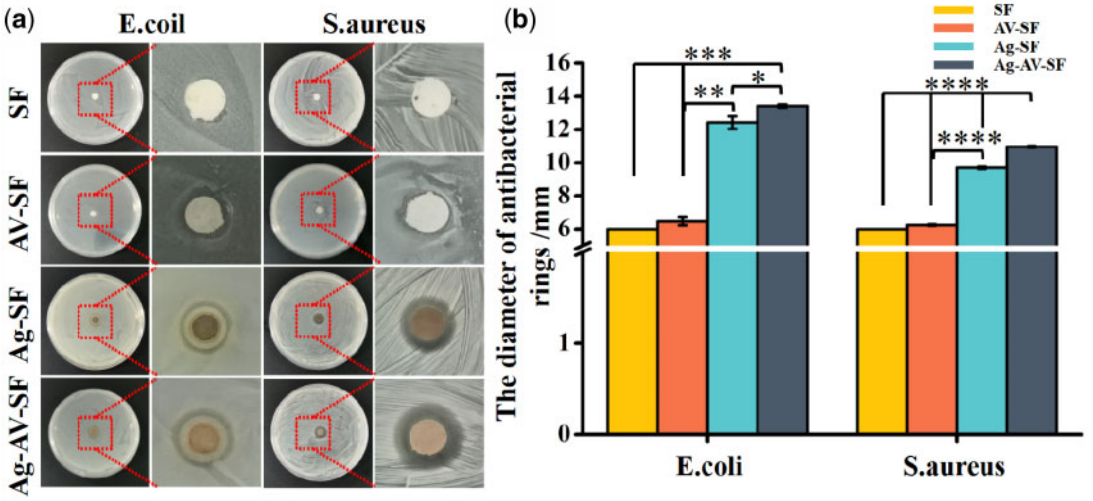

Figure 4. The antibacterial properties of the four hydrogels. (a) The Ag–AV–SF hydrogel showed the largest diameter of the antibacterial rings for both *E. coli* and *S. aureus*; (b) the Ag–AV–SF hydrogel showed significant difference with other single modifiers based hydrogel for both anti-*E. coli* and anti-*S. aureus* performance (*$P < 0.05$, **$P < 0.01$, ***$P < 0.001$, ****$P < 0.0001$)

which is more than the blank control group (86.47%), SF hydrogel-treated group (88.99%), AV–SF hydrogel-treated group (93.66%) and Ag–SF hydrogel-treated group (92.74%). The results show that the Ag–AV–SF hydrogel performs excellently both in the early inflammatory response stages and in the subsequent stages of tissue repair, regeneration and remodeling.

To further verify its healing efficacy, SS cream, a wound dressing currently on sale [36], was selected as the contrast dressing. The wounds are shown in Fig. 7a, the area recorded and calculated on the 0th, 7th, 14th and 21st day (Fig. 7b). The areas show no significant differences at the beginning. On Day 7, the area of the Ag–AV–SF-treated groups showed the maximum reduction in area. On Day 14, the group treated with Ag–AV–SF hydrogel decreased more than other groups. On Day 21, the extent of the wound treated with the Ag–AV–SF hydrogel was nearly completely closed and the healing rate reached 97.02%. It is worth

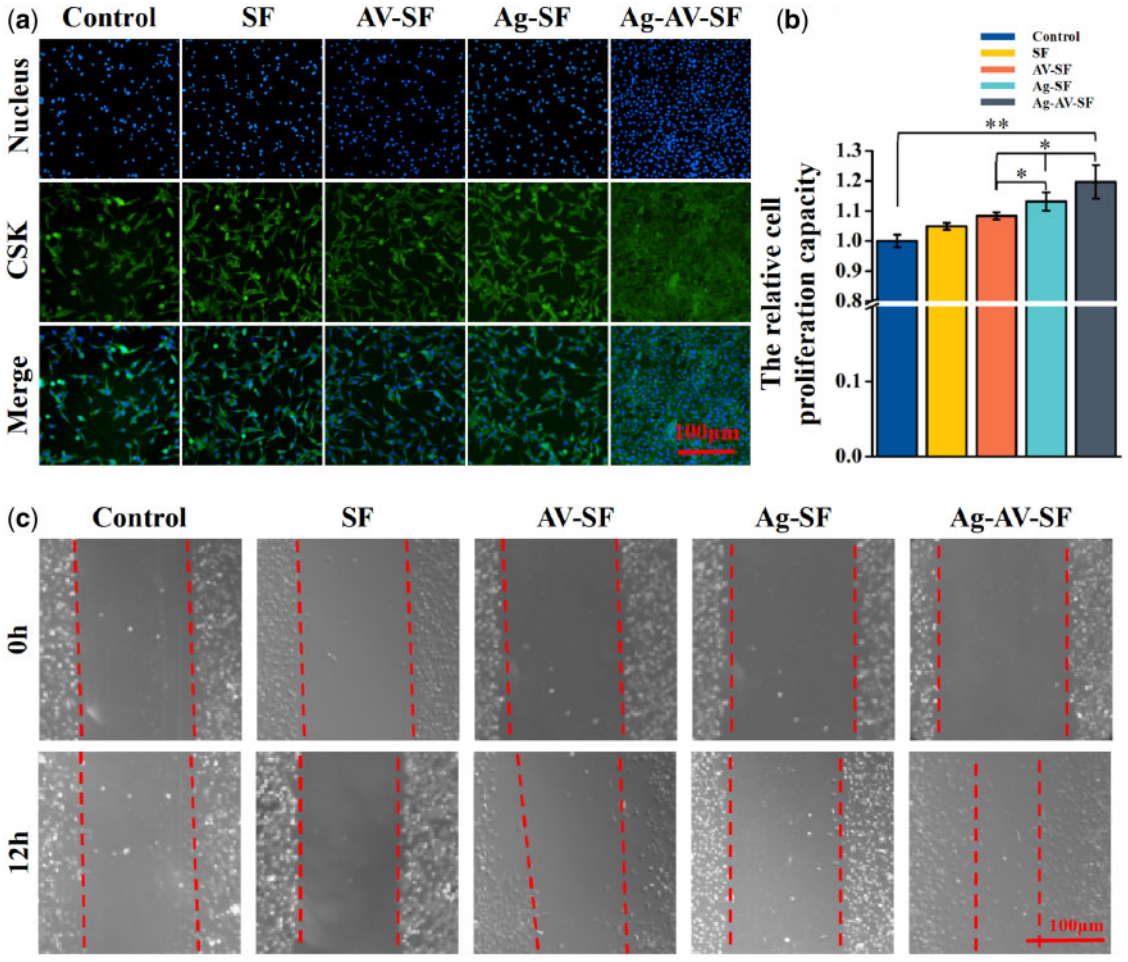

Figure 5. Proliferation and migration assays of L929 *in vitro* and diffusion *in vivo*: (a) fluorescence staining of cell proliferation, (b) CCK-8 assay and (c) scratch test (*$P < 0.05$, **$P < 0.01$)

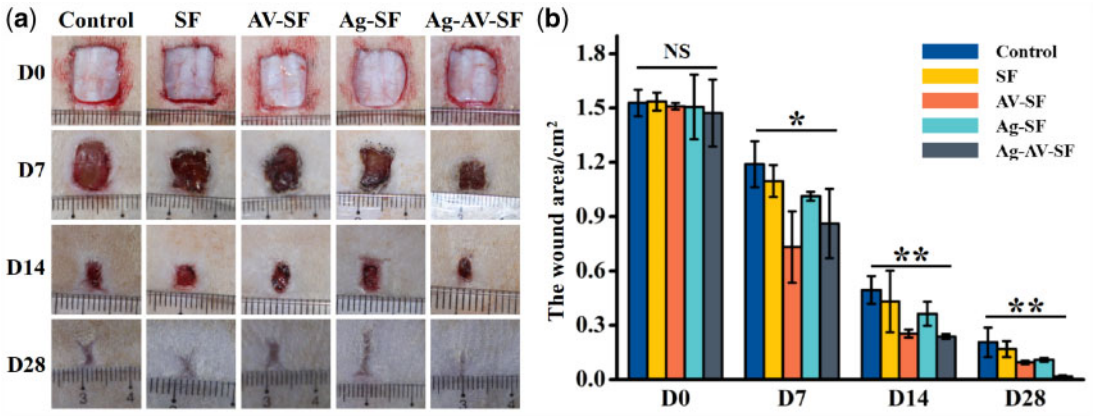

Figure 6. Photographs of the wound healing status after the injection of normal saline (control), SF-hydrogel, AV–SF hydrogel, Ag–AV–SF hydrogel and Ag–AV–SF hydrogel: (a) extent of the wound regenerating area on Days 0, 7, 14 and 28 after surgery, (b) the statistical analysis of the wound area (NS: non-significant; *$P < 0.05$, **$P < 0.01$)

noting that wound healing in rats was achieved by wound contraction and not by reepithelialization [37]. The Ag–AV–SF hydrogel effectively promoted the wound contraction, making the healing rates significantly higher than other groups. Meanwhile, the Ag–AV–SF hydrogel-treated group showed less formation of scar tissue on the 7th and 21st day. The results revel that the Ag–AV–SF hydrogel performed excellently both in promoting healing and inhibiting the formation of a scar.

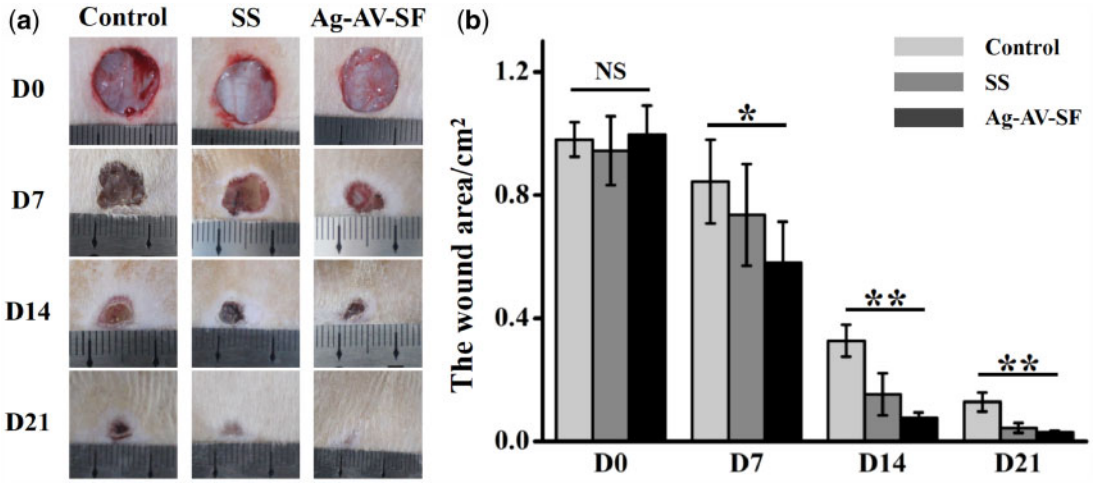

Figure 7. Photographs of the wound healing status after the injection of normal saline (control), sulfadiazine silver cream and Ag–AV–SF hydrogel: (a) extent of the wound regenerating area on Days 0, 7, 14 and 21 after surgery, (b) the statistical analysis of the wound area (NS: non-significant, $*P < 0.05$, $**P < 0.01$)

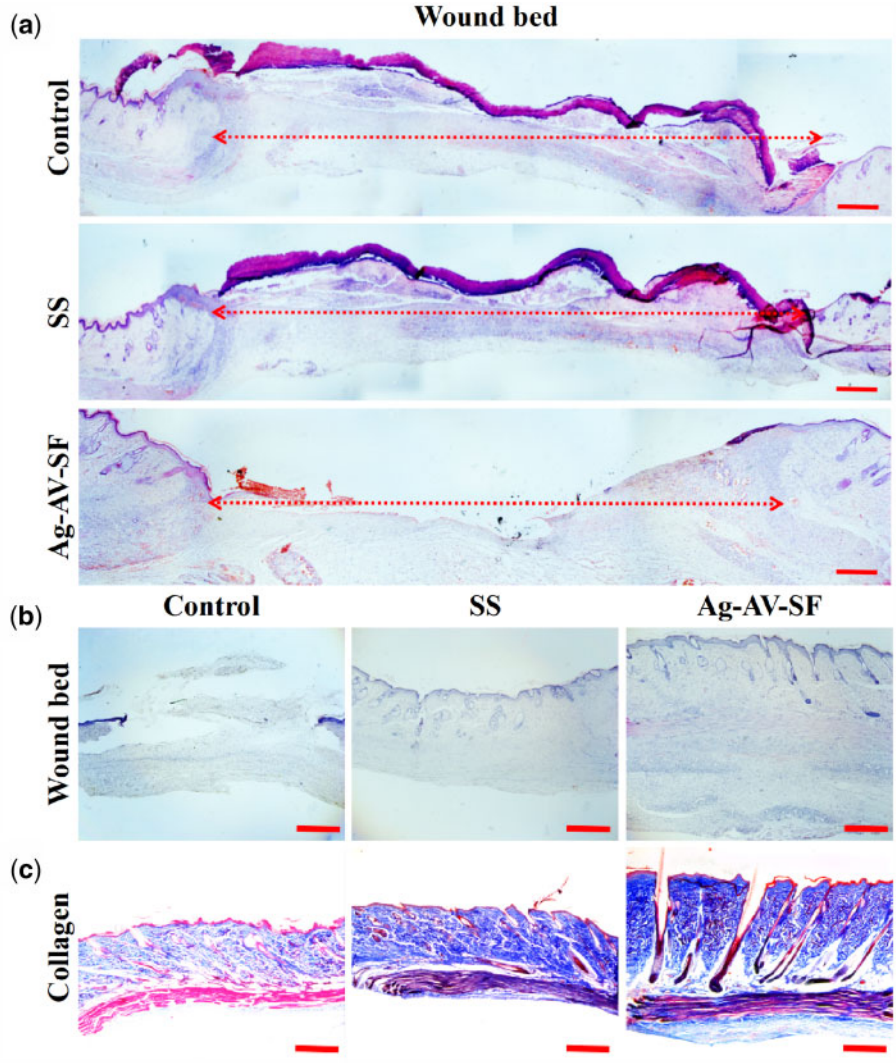

Figure 8. The wound bed and collagen deposition of the wound (a and b) Ag–AV–SF hydrogel induced the most contrast of the wound bed on both Day 7 (scale bar 500 μm) and Day 21 (scale bar 200 μm), (c) the collagen deposition on Day 21 (scale bar 200 μm)

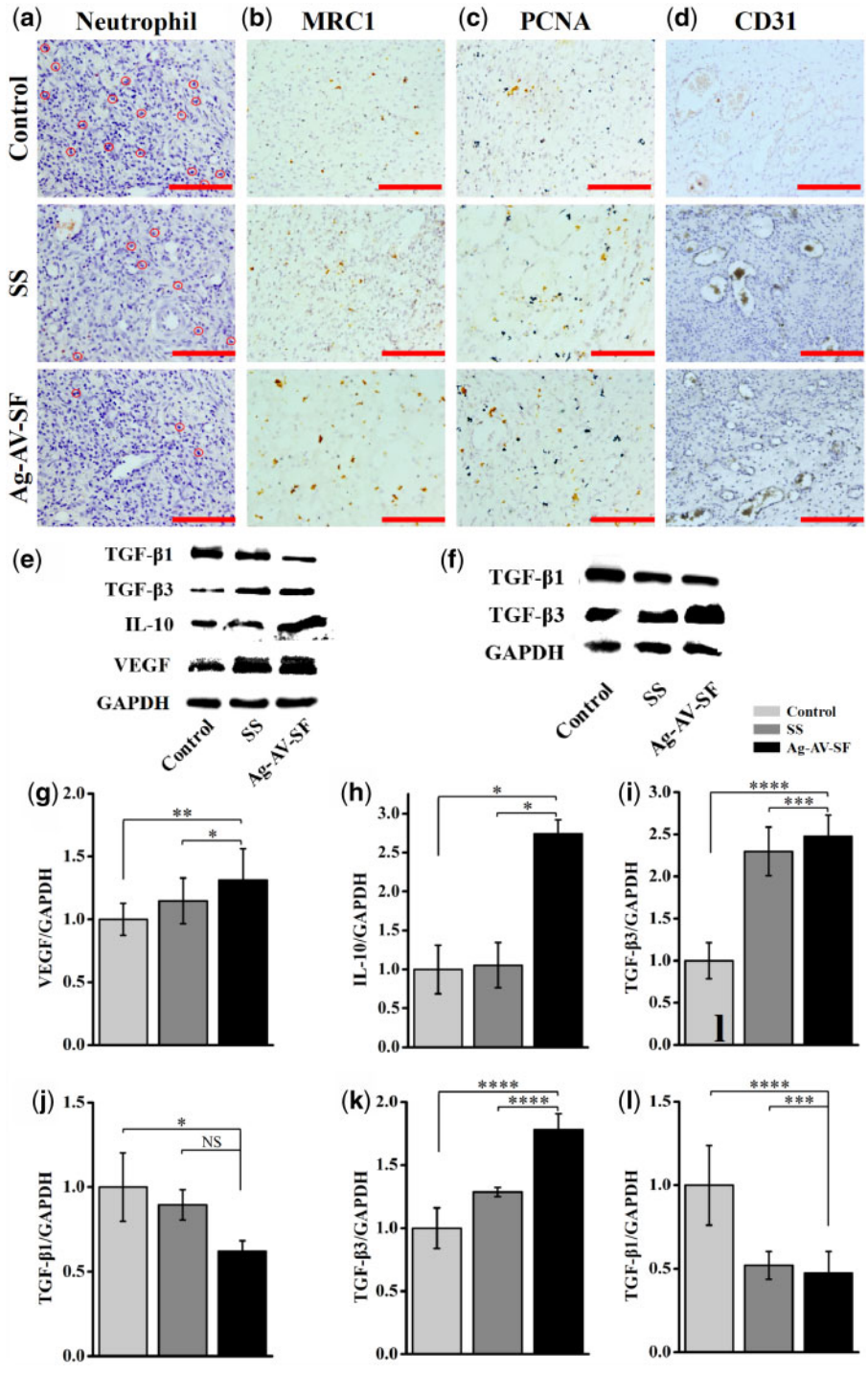

Figure 9. The neutrophil and immunohistochemical staining on Day 7 and the protein expression level on Days 7 and 21 of the control, SS and Ag–AV–SF-treated groups: (a) the neutrophil on the wound, (b–d) the immunohistological staining for MRC1, PCNA and CD31, (e, g–j) the expression level of TGF-β1, TGF-β3, IL-10 and VEGF on Day 7, (f, k and l) the expression level of TGF-β1, TGF-β3 on Day 21 (NS: non-significant, $*P<0.05$, $**P<0.01$, $***P<0.001$, $****P<0.0001$)

Histological analysis

To evaluate the outstanding effects of Ag–AV–SF hydrogel, the IHC staining for CD68, HE staining and Masson staining were employed and the results showed that the effects of Ag–AV–SF hydrogel are better than the single modifiers hydrogel (Fig. S3).

HE staining of the wound tissue on the 7th day showed that the wound bed of the Ag–AV–SF hydrogel-treated group is the shortest compared with the other groups (Fig. 8a). The HE staining on Day 21 showed that the skin structure of the Ag–AV–SF hydrogel-treated group is more complete than other processing groups (Fig. 8b). Collagen deposition is more beneficial for tissue reconstruction. Masson staining of the wound on Day 21 showed that the Ag–AV–SF hydrogel promoted the collagen deposition on the wound (Fig. 8c).

The HE staining of the wound sites showed the amounts of neutrophils on Day 7. As shown in Fig. 9a, the Ag–AV–SF hydrogel-

Table 1. Comparison of materials forms, methods, and efficacy with other biomaterials used in the treatment of cutaneous wounds

Materials	Forms	Method	Effects	Year	References
VSFNPs	Scaffolds	Chemical crosslinking	Inhibit bone infections and drug slow release	2017	[54]
PEGS–FA	Hydrogel	Chemical crosslinking	*In vivo* blood clotting, antibacterial, anti-oxidant and electroactive dressing	2017	[55]
SF	Scaffolds	Lyophilization	Promote neovascularization and cell migration	2018	[5]
SF	Hydrogel	Self-assembly	Promote proliferation of fibroblasts and migration of keratinocytes	2018	[56]
MHA/TPEG	Hydrogel	Photopolymerization	–	2018	[57]
PAF	Films	Chemical crosslinking	Promoted the epithelialization and well-organized collagen deposition	2019	[58]
GT–DA/CHI/CNT	Hydrogel	Chemical crosslinking	Hemostatic, antioxidant and antimicrobial	2019	[59]
QHM	Hydrogel	Chemical crosslinking	Hemostasis and antibacterial	2019	[60]
SF/FGF1	Hydrogel	Sonication	Promote the wound healing	2019	[12]
BC–MMT–Ag	Hydrogel	Chemical crosslinking	Inhibit growth in agar plates and biofilm formation	2020	[61]
DABH	Hydrogel	Chemical crosslinking	Hemostasis and wound healing.	2020	[62]
MHA/MaPVA	Nanofibers Membrane	Photocrosslinking	Promote the cell attachment	2019	[63]
ACC@Fe2+/BML-CaSi-GP	Scaffolds	Chemical crosslinking	Antitumor and tissue repair	2021	[64]
Ag–AV–SF	Hydrogel	Photocrosslinking	Promote the cell proliferation and migration, inhibit the immune reaction.	2021	This work

treated group has the lowest density of neutrophil. The IHC for MRC1 on the 7th day marked the M2 macrophages which benefit wound healing. In Fig. 9b, the Ag–AV–SF hydrogel-treated group had the highest density of the right immune cells. Moderate immune response on local wounds during the early stages of healing induce reactive neovascularization, improving the recovery of the vessel network and the removal of lesion metabolism products, hastening wound closure. PCNA is a key factor to assess cell proliferation ability *in vivo*. The IHC for PCNA of the wound sites on the 7th day reflected that the Ag–AV–SF hydrogel induced the most cell proliferation at the beginning of healing (Fig. 9c). The IHC for CD31 on the 7th day reflected the revascularization of the wound sites. The densities of newly developed blood vessels treated with Ag–AV–SF hydrogel were higher than those of the other groups, which could be attributed to the mild immune response caused by reactive blood vessel regeneration (Fig. 9d).

Effects of different treatments on VEGF, IL-10, TGF-β1 and TGF-β3 levels

The expression levels of VEGF, IL-10, TGF-β1 and TGF-β3 in skin tissue were detected using western blotting. The Ag–AV–SF hydrogel increased the expression of VEGF, indicating the hydrogel benefits the angiogenesis on the 7th day (Fig. 9e and g). On the 7th day, the Ag–AV–SF hydrogel upregulated IL-10 compared with the other groups (Fig. 9e and h), suggesting the prepared hydrogel promoted the macrophage transformation from the M1 phenotype to M2 at the early stage of healing. On Days 7 and 21 post-surgery, the relative expression level of TGF-β1 and TGF-β3 showed an opposite trend, the Ag–AV–SF hydrogel upregulated the expression of TGF-β3 and downregulated the expression of TGF-β1, which means the prepared hydrogel shows the capacities to inhibit scar formation (Fig. 9e, i, j, f, k and l).

Reliable biosecurity of different hydrogels

The accumulation of AgNPs is the main reason for its cytotoxic behavior, along with its damage to tissues and organs. So, we operated the diffusion range test. The diffusion ranges of the hydrogel after treated for 0, 4, 12 and 24 h were recorded in Fig. S4a–d. Instead of spreading throughout the body, the hydrogel remained relatively immobilized at the site of the wound, ensuring that AgNPs are immobilized locally to the wound to avoid systemic toxicity. The subsequent HE results showed that the structure of heart, brain, spleen, lung, testis, kidney and liver were complete, and there was no significant pathological change caused by the deposition of metal particles. For the liver, as the most important toxic metabolic organ, there was no obvious pathological change in the liver tissue by HE staining, implying the Ag–AV–SF hydrogel will cause any damage to organs (Fig. S5).

Discussion

Skin defect is a major clinical concern, and incorrect treatments will cause irreversible damage. Therefore, creating a wound dressing with excellent bioactivity is crucial.

Recent years have witnessed the wide use of hydrogels for wound healing, along with the development of many approaches to fabricating hydrogels (Table 1). Among them, chemical crosslinking is the most common strategy. Comparatively, photocrosslinking avoids unpredictable biological toxicity or other side effects caused by the introduction of crosslinking agents, and is a safer, green and environmentally friendly method. In addition, the accumulation of AgNPs is the main reason for its cytotoxic behavior, along with its damage to tissues and organs. The potential transfer of silver deposits to the brain and the lung should be considered, as the AgNPs can cross various biological barriers and enter the circulatory system [38]. All the components in this study are natural biomaterials and no chemical crosslinking agent was introduced, so the hydrogel kept its biological activity close to the original state, ensuring its biological safety in application. The biosecurity evaluation of Ag–AV–SF hydrogel revealed the good biocompatibility *in vivo*.

In addition to the safe and green approach, the Ag–AV–SF hydrogel also acted as a compound system that exhibited better effect on both antibacterial properties and wound healing on the immunological level. An open wound provides adhesion sites for bacteria to infiltrate and reproduce, significantly increasing the risk of infection. Excessive inflammation causes prolonged release of inflammatory

cytokines and the activation of immune complexes, thus impairing cutaneous wound healing [39]. The hydrogel exhibited good antibacterial properties according to the results from the antibacterial rings (Fig. 4). Furthermore, the acidic-pH-responsive property ensures that the prepared hydrogel release more AgNPs in chronic wound environment and it was studied that the higher percentage of silver induce less macrophage and result in lower immunoreaction level [17]. In comparison with the single modifiers, the Ag–AV–SF hydrogel induced the weakest immune response at the early stage. Neutrophils in a wound eliminate pathogens by phagocytosis and release the bactericidal reactive oxygen species and peptides [40]. Ag–AV–SF hydrogel induced the lowest neutrophils level meaning that the hydrogel showed better anti-inflammatory activity than SS (Fig. 9a). More interestingly, macrophages immunologically can be classified as classically activated (M1) and alternatively activated (M2) cells, or M2-like types. The M2 macrophages release the IL-10, which promotes wound healing [41]. Relatively higher expression levels of IL-10 (Fig. 9e and h) and the results of IHC staining for MRC1 (Fig. 9b) verified that the prepared hydrogel promoted transformation from M1 to M2.

Noteworthily, contraction is the major wound healing mechanism in rodents [42], and cell proliferation and migration are the fundamentals of wound healing. Fibroblasts are a type of skin cell more closely associated with skin and wound healing than MSCs [29], and also play significant roles during the proliferation phase, infiltrating the wound sites to produce extracellular compounds, which forms the basis of granulation tissue [43]. SF was proven to promote wound healing by activating Protein Kinase B mammalian Target of Rapamycin (AKT/mTOR) signaling and mitogen-activated protein kinase signaling, along with the inactivation of the apoptotic pathway. It was further proven that SF stimulates cell migration through the activation of c-Jun N-terminal kinases 1/2 and extracellular signal-regulated kinases 1/2 [44, 45]. Complementarily, the mannose-6-phosphate in AV affects the fibroblast growth factor and stimulates the activity and proliferation of fibroblasts, promoting wound healing [46]. Furthermore, Kumar *et al.* concluded that the highest percentage of silver induced the smallest wound area, few macrophages and more fibroblasts via treating the wounded rats using creams with different concentrations of AgNPs [17]. In current study, the Ag–AV–SF hydrogel-treated group presented greatly increasing cell proliferation both *in vivo* and *in vitro* (Figs 5a and b and 9c), effectively reducing the wound area. More deeply, neovascularization could efficiently deliver nutrients to granulation tissue for filling the wound defect [47]. In this composite system, SF accelerates wound healing by regulating (Nuclear Factor kappa-B)NF-κB modulated proteins, such as (Vascular Endothelial Growth Factors)VEGFs [48]. For AV, it could directly interact with the vascular endothelial cells and release VEGF to ameliorate angiogenesis *in vivo* through the promotion of cell proliferation, besides, relative studies also found that the β-sitosterol in AV can improve angiogenesis by increasing the expression of VEGF and its receptors at wound sites [49]. In our study, the Ag–AV–SF hydrogel exhibited superior functionality in terms of the reconstruction of blood-vessel networks according to the IHC for CD31 (Fig. 9d) and the highest expression of VEGF over the other experimental groups (Fig. 9e and g). Overall, the Ag–AV–SF hydrogel is synergistic with the excellent bioactivity of internal components, presenting proliferation- and migration-promoting capacities both *in vitro* and *in vivo*, meanwhile, effectively promotes angiogenesis thus accelerating the remodeling of vascular networks and performing better effects than wound dressings based on single modifiers and SS.

Scars are inevitable results of surgical procedures, and their prevention is still a major problem in the field of cosmetic surgery [50]. More importantly, the balance between the four primary steps of wound healing determines the dynamics of regeneration, and the outcome of wound healing, in particular, scar formation [51]. TGF-β1 and TGF-β3 play inverse roles in the formation of scars. TGF-β3 was reported to be a potential anti-scarring therapy according to clinical trials [52], while the TGF-β1 protein levels of hypertrophic scars tended to increase with increasing severity of the scars [53]. According to the protein expression level, Ag–AV–SF hydrogel upregulates the expression of TGF-β3 and downregulates the expression of TGF-β1 (Fig. 9e and f), intuitively reducing the formation of scars (Fig. 7a). The Ag–AV–SF hydrogel prepared in the study is expected to provide a potential therapeutic option for scarless wound healing.

Conclusion

In this study, Ag–AV–SF hydrogel combined the comprehensive properties of AgNPs and AV, developed using a 'green' (environmentally friendly) photocrosslinking approach. In comparison with both single-modifier hydrogels and the wound dressings currently on sale, the Ag–AV–SF hydrogel fabricated herein inhibited immune reactions and promoted the healing process. In the histological analysis, the Ag–AV–SF hydrogel induced a mild immune reaction and enhanced neovascularization. More interestingly, it induced the macrophage transformation from the M1 phenotype to M2 at the early stage of healing. Additionally, it upregulated the expression of TGF-β3 and downregulated the expression of TGF-β1, thus reducing the formation of scar tissue. It is believed that the Ag–AV–SF hydrogel will function as a promising wound dressing to address future clinical wound problems.

Conflict of Interest statement

There is no conflict of interest

Supplementary data

Supplementary data are available at *REGBIO* online.

Funding

This work was supported by the National Natural Science Foundation of China (12032007, 31971242); the Natural Science Foundation of Chongqing (cstc2020jcyj-msxmX0330); the Project of Science and Technology of Chongqing Yuzhong District (20170119, 20170113), the Project of Tutorial System of Medical Undergraduate in Lab Teaching & Management Center in Chongqing Medical University (LTMCMTS202003), the National Project of University Students Innovation and Entrepreneurship Training Program (201910631002), the Project of 'Ying Yao Program' for College Student in School of Basic Medical Sciences in Chongqing Medical University(JCYY202003).

References

1. Falanga V. Wound healing and its impairment in the diabetic foot. *Lancet* 2005;**366**:1736–43.
2. Gilotra S, Chouhan D, Bhardwaj N *et al.* Potential of silk sericin based nanofibrous mats for wound dressing applications. *Mater Sci Eng C Mater Biol Appl* 2018;**90**:420–32.
3. Gil ES, Panilaitis B, Bellas E *et al.* Functionalized silk biomaterials for wound healing. *Adv Healthc Mater* 2013;**2**:206–17.

4. Eming SA, Martin P, Tomic-Canic M. Wound repair and regeneration: mechanisms, signaling, and translation. *Sci Transl Med* 2014;**6**:265sr6.
5. Lu G, Ding Z, Wei Y *et al.* Anisotropic biomimetic silk scaffolds for improved cell migration and healing of skin wounds. *ACS Appl Mater Interfaces* 2018;**10**:44314–23.
6. Mir M, Ali MN, Barakullah A *et al.* Synthetic polymeric biomaterials for wound healing: a review. *Prog Biomater* 2018;**7**:1–21.
7. Huang Y, Zhao X, Zhang Z *et al.* Degradable gelatin-based IPN cryogel hemostat for rapidly stopping deep noncompressible hemorrhage and simultaneously improving wound healing. *Chem Mater* 2020;**32**:6595–610.
8. Lovett M, Cannizzaro C, Daheron L *et al.* Silk fibroin microtubes for blood vessel engineering. *Biomaterials* 2007;**28**:5271–9.
9. Hopkins AM, De Laporte L, Tortelli F *et al.* Silk hydrogels as soft substrates for neural tissue engineering. *Adv Funct Mater* 2013;**23**:5140–9.
10. Zhang F, You X, Dou H *et al.* Facile fabrication of robust silk nanofibril films via direct dissolution of silk in CaCl2-formic acid solution. *ACS Appl Mater Interfaces* 2015;**7**:3352–61.
11. Kapoor S, Kundu SC. Silk protein-based hydrogels: promising advanced materials for biomedical applications. *Acta Biomater* 2016;**31**:17–32.
12. He S, Shi D, Han Z *et al.* Heparinized silk fibroin hydrogels loading FGF1 promote the wound healing in rats with full-thickness skin excision. *Biomed Eng Online* 2019;**18**:97.
13. Jing J, Liang S, Yan Y *et al.* Fabrication of hybrid hydrogels from silk fibroin and tannic acid with enhanced gelation and antibacterial activities. *ACS Biomater Sci Eng* 2019;**5**:4601–11.
14. Wang SD, Ma Q, Wang K *et al.* Improving antibacterial activity and biocompatibility of bioinspired electrospinning silk fibroin nanofibers modified by graphene oxide. *ACS Omega* 2018;**3**:406–13.
15. Tang S, Zheng J. Antibacterial activity of silver nanoparticles: structural effects. *Adv Healthc Mater* 2018;**7**:e1701503.
16. Calamak S, Aksoy EA, Ertas N *et al.* Ag/silk fibroin nanofibers: effect of fibroin morphology on Ag+ release and antibacterial activity. *Eur Polym J* 2015;**67**:99–112.
17. Kumar SSD, Rajendran NK, Houreld NN *et al.* Recent advances on silver nanoparticle and biopolymer-based biomaterials for wound healing applications. *Int J Biol Macromol* 2018;**115**:165–75.
18. Xu H-L, Chen P-P, Wang L-f *et al.* Hair regenerative effect of silk fibroin hydrogel with incorporation of FGF-2-liposome and its potential mechanism in mice with testosterone-induced alopecia areata. *J Drug Deliv Sci Technol* 2018;**48**:128–36.
19. Maenthaisong R, Chaiyakunapruk N, Niruntraporn S *et al.* The efficacy of aloe vera used for burn wound healing: a systematic review. *Burns* 2007;**33**:713–8.
20. Tamahkar E, Özkahraman B, Özbaş Z *et al.* Aloe vera-based antibacterial porous sponges for wound dressing applications. *J Porous Mater* 2021;**28**:741–50.
21. Singh S, Gupta A, Gupta B *et al.* Scar free healing mediated by the release of aloe vera and manuka honey from dextran bionanocomposite wound dressings. *Int J Biol Macromol* 2018;**120**:1581–90.
22. Kim DH, Viventi J, Amsden JJ *et al.* Dissolvable films of silk fibroin for ultrathin conformal bio-integrated electronics. *Nat Mater* 2010;**9**:511–7.
23. Vieira D, Angel S, Honjol Y *et al.* Electroceutical silk–silver gel to eradicate bacterial infection. *Adv Biosyst* 2020;**4**:e1900242.
24. Nejaddehbashi F, Hashemitabar M, Bayati V *et al.* Incorporation of silver sulfadiazine into an electrospun composite of polycaprolactone as an antibacterial scaffold for wound healing in rats. *Cell J* 2020;**21**:379–90.
25. Qian B, Li J, Guo K *et al.* Antioxidant biocompatible composite collagen dressing for diabetic wound healing in rat model. *Regen Biomater* 2021;**8**:rbab003.
26. Yuk H, Varela CE, Nabzdyk CS *et al.* Dry double-sided tape for adhesion of wet tissues and devices. *Nature* 2019;**575**:169–74.
27. Hunt CA, Macgregor RD, Siegel RA. Engineering targeted in vivo drug delivery. I. The physiological and physicochemical principles governing opportunities and limitations. *Pharm Res* 1986;**3**:333–44.
28. Liang Y, Zhao X, Hu T *et al.* Adhesive hemostatic conducting injectable composite hydrogels with sustained drug release and photothermal antibacterial activity to promote full-thickness skin regeneration during wound healing. *Small* 2019;**15**:e1900046.
29. Li B, Wang JH-C. Fibroblasts and myofibroblasts in wound healing: force generation and measurement. *J Tissue Viability* 2011;**20**:108–20.
30. Pan Y, Zhao Y, Kuang R *et al.* Injectable hydrogel-loaded nano-hydroxyapatite that improves bone regeneration and alveolar ridge promotion. *Mater Sci Eng C Mater Biol Appl* 2020;**116**:111158.
31. Martinotti S, Ranzato E. Scratch wound healing assay. *Methods Mol Biol* 2020;**2109**:225–9.
32. Pirkmajer B, Leusch G. A bladder-prostate model on which to practice using transurethral resection instruments (author's transl). *Urologe A* 1977;**16**:336–8.
33. Maddinedi SB, Mandal BK, Anna KK. Tyrosine assisted size controlled synthesis of silver nanoparticles and their catalytic, in-vitro cytotoxicity evaluation. *Environ Toxicol Pharmacol* 2017;**51**:23–9.
34. Zhang R, Han Q, Li Y *et al.* High antibacterial performance of electrospinning silk fibroin/gelatin film modified with graphene oxide-sliver nanoparticles. *J Appl Polym Sci* 2019;**136**:47904.
35. Sato K, Asai T, Jimi TS. Collagen-derived di-peptide, prolylhydroxyproline (pro-hyp): a new low molecular weight growth-initiating factor for specific fibroblasts associated with wound healing. *Front Cell Dev Biol* 2020;**8**:548975.
36. Naseri-Nosar M, Ziora ZM. Wound dressings from naturally-occurring polymers: a review on homopolysaccharide-based composites. *Carbohydr Polym* 2018;**189**:379–98.
37. Gurtner GC, Werner S, Barrandon Y *et al.* Wound repair and regeneration. *Nature* 2008;**453**:314–21.
38. Ferdous Z, Nemmar A. Health impact of silver nanoparticles: a review of the biodistribution and toxicity following various routes of exposure. *Int J Mol Sci* 2020;**21**:2375.
39. Leaper D, Assadian O, Edmiston CE. Approach to chronic wound infections. *Br J Dermatol* 2015;**173**:351–8.
40. Brinkmann V, Reichard U, Goosmann C *et al.* Neutrophil extracellular traps kill bacteria. *Science* 2004;**303**:1532–5.
41. Zhang W, Qi X, Zhao Y *et al.* Study of injectable Blueberry anthocyaninsloaded hydrogel for promoting full-thickness wound healing. *Int J Pharm* 2020;**586**:119543.
42. Nuutila K, Singh M, Kruse C *et al.* Titanium wound chambers for wound healing research. *Wound Repair Regen* 2016;**24**:1097–102.
43. Tomasek JJ, Gabbiani G, Hinz B *et al.* Myofibroblasts and mechanoregulation of connective tissue remodelling. *Nat Rev Mol Cell Biol* 2002;**3**:349–63.
44. Martinez-Mora C, Mrowiec A, Garcia-Vizcaino EM *et al.* Fibroin and sericin from Bombyx mori silk stimulate cell migration through upregulation and phosphorylation of c-Jun. *PLoS One* 2012;**7**:e42271.
45. Sultan MT, Lee OJ, Kim SH *et al.* Silk fibroin in wound healing process. *Adv Exp Med Biol* 2018;**1077**:115–26.
46. Hashemi SA, Madani S, Abediankenari AS. The review on properties of aloe vera in healing of cutaneous wounds. *Biomed Res Int* 2015;**2015**:714216.
47. Greaves NS, Ashcroft KJ, Baguneid M *et al.* Current understanding of molecular and cellular mechanisms in fibroplasia and angiogenesis during acute wound healing. *J Dermatol Sci* 2013;**72**:206–17.
48. Nam YS, Yoon JJ, Park TG. A novel fabrication method of macroporous biodegradable polymer scaffolds using gas foaming salt as a porogen additive. *J Biomed Mater Res* 2000;**53**:1–7.
49. Moon EJ, Lee YM, Lee OH *et al.* A ncovel angiogenic factor derived from aloe vera gel: β-sitosterol, a plant sterol. *Angiogenesis* 1999;**3**:117–23.
50. Abedini R, Rayeni NM, Abianeh SH *et al.* Botulinum toxin type A injection for mammoplasty and abdominoplasty scar management: a split-scar double-blinded randomized controlled study. *Aesthetic Plast Surg* 2020;**44**:2270–6.
51. Nosenko MA, Moysenovich AM, Zvartsev RV *et al.* Novel biodegradable polymeric microparticles facilitate scarless wound healing by promoting re-epithelialization and inhibiting fibrosis. *Front Immunol* 2018;**9**:2851.

52. Ferguson MWJ, Duncan J, Bond J *et al.* Prophylactic administration of avotermin for improvement of skin scarring: three double-blind, placebo-controlled, phase I/II studies. *Lancet* 2009;**373**:1264–74.
53. Kim SY, Seung MN, Park ES *et al.* Differences in hypertrophic scar fibroblasts according to scar severity: expression of transforming growth factor β1 at the mRNA and protein levels. *Arch Aesthetic Plast Surg* 2015;**21**:116–20.
54. Besheli NH, Mottaghitalab F, Eslami M *et al.* Sustainable release of vancomycin from silk fibroin nanoparticles for treating severe bone infection in rat tibia osteomyelitis model. *ACS Appl Mater Interfaces* 2017;**9**:5128–38.
55. Zhao X, Wu H, Guo B *et al.* Antibacterial anti-oxidant electroactive injectable hydrogel as self-healing wound dressing with hemostasis and adhesiveness for cutaneous wound healing. *Biomaterials* 2017;**122**:34–47.
56. Chouhan D, Lohe TU, Samudrala PK *et al.* In situ forming injectable silk fibroin hydrogel promotes skin regeneration in full thickness burn wounds. *Adv Healthcare Mater* 2018;**7**:1801092.
57. Zhang C, Dong Q, Liang K *et al.* Photopolymerizable thiol-acrylate maleiated hyaluronic acid/thiol-terminated poly(ethylene glycol) hydrogels as potential in-situ formable scaffolds. *Int J Biol Macromol* 2018;**119**:270–7.
58. Wang J, Chen Y, Zhou G *et al.* Polydopamine-coated *Antheraea pernyi* (*A. pernyi*) silk fibroin films promote cell adhesion and wound healing in skin tissue repair. *ACS Appl Mater Interfaces* 2019;**11**:34736–43.
59. Liang Y, Zhao X, Hu T *et al.* Mussel-inspired, antibacterial, conductive, antioxidant, injectable composite hydrogel wound dressing to promote the regeneration of infected skin. *J Colloid Interface Sci* 2019;**556**:514–28.
60. Wang C, Niu H, Ma X *et al.* Bioinspired, injectable, quaternized hydroxyethyl cellulose composite hydrogel coordinated by mesocellular silica foam for rapid, noncompressible hemostasis and wound healing. *ACS Appl Mater Interfaces* 2019;**11**:34595–608.
61. Horue M, Cacicedo ML, Fernandez MA *et al.* Antimicrobial activities of bacterial cellulose – silver montmorillonite nanocomposites for wound healing. *Mater Sci Eng C Mater Biol Appl* 2020;**116**:111152.
62. Han W, Zhou B, Yang K *et al.* Biofilm-inspired adhesive and antibacterial hydrogel with tough tissue integration performance for sealing hemostasis and wound healing. *Bioact Mater* 2020;**5**:768–78.
63. Chen X, Lu B, Zhou D *et al.* Photocrosslinking maleilated hyaluronate/methacrylated poly (vinyl alcohol) nanofibrous mats for hydrogel wound dressings. *Int J Biol Macromol* 2020;**155**:903–10.
64. Xue CC, Li MH, Sutrisno L *et al.* Bioresorbable scaffolds with biocatalytic chemotherapy and in situ microenvironment modulation for postoperative tissue repair. *Adv Funct Mater* 2021;**31**:2008732.